The Histone H1-like protein AlgP facilitates even spacing of polyphosphate granules in *Pseudomonas aeruginosa*

Ravi Chawla[*,a], Steven Klupt[*,b], Vadim Patsalo[a], James R Williamson[a], Lisa R Racki[a,†]

*****Ravi Chawla and Steven Klupt contributed equally to this work. Author order was determined alphabetically*

Affiliations:

[a]Department of Integrative Structural and Computational Biology, Scripps Research, La Jolla, CA

[b]Department of Immunology and Microbiology, Scripps Research, La Jolla, CA

[†]Correspondence to: lracki@scripps.edu

ABSTRACT

Synthesis of polyphosphate (polyP) is an ancient and universal stress and starvation response in bacteria. In many bacteria, polyP chains come together to form granular superstructures within cells. Some species appear to regulate polyP granule subcellular organization. Despite the critical role of polyP in starvation fitness, the composition of these structures, mechanism(s) underpinning their organization, and functional significance of such organization are poorly understood. We previously determined that granules become transiently evenly spaced on the cell's long axis during nitrogen starvation in the opportunistic human pathogen *Pseudomonas aeruginosa*. Here, we developed a granule-enrichment protocol to screen for polyP granule-localizing proteins. We identified AlgP as a protein that associates with polyP granules. We further discovered that AlgP is required for the even spacing of polyP granules. AlgP is a DNA-binding protein with a 154 amino acid C-terminal domain enriched in 'KPAA' repeats and variants of this repeat, with an overall sequence composition similar to the C-terminal tail of eukaryotic histone H1. Granule size, number, and spacing are significantly perturbed in the absence of AlgP, or when AlgP is truncated to remove the C-terminus. The Δ*algP* and *algP*ΔCTD mutants having fewer, larger granules. We speculate that AlgP may contribute to spacing by tethering polyP granules to the chromosome, thereby inhibiting fusion with neighboring granules. Our discovery that AlgP facilitates granule spacing allows us for the first time to directly uncouple granule biogenesis from even spacing, and will inform future efforts to explore the functional significance of granule organization on fitness during starvation.

IMPORTANCE

The mechanisms underpinning polyP's pleiotropic effects on bacterial starvation physiology remain elusive. This simple polyanion's lack of protein binding specificity has impeded validation of *bona fide* polyP-binding proteins. However, polyP forms granule superstructures with spatial specificity. Our granule enrichment protocol identified a polyP granule-associated protein in *Pseudomonas*

aeruginosa, AlgP. AlgP was originally reported as regulator of alginate, an extracellular polysaccharide important in biofilm formation, including in cystic fibrosis (CF) chronic infections. AlgP's putative role in alginate biosynthesis has recently been called into question. We establish a distinct, previously unknown function for AlgP in modulating the subcellular organization of polyP, another polymer important for pathogenesis. In CF clinical isolates, the C-terminal repeat domain of AlgP is a hotspot for genetic rearrangements. Our finding that the C-terminus of AlgP is required for granule organization lays the groundwork for exploring the functional significance of these mutations in the evolutionary trajectory of chronic infections.

INTRODUCTION

In response to diverse starvation cues, bacteria almost universally do a curious thing: They spend ATP to make an inorganic polymer of phosphoryl groups, polyphosphate (polyP). The ability to make polyP has been shown to be important for fitness during starvation in evolutionarily disparate bacterial species, but the molecular mechanism(s) underpinning these effects has remained mysterious(1, 2). A significant challenge to understanding how polyP exerts its pleiotropic effects on physiology has been the small number of validated polyP-binding proteins identified in bacteria. Aside from the polyP biosynthetic machinery (kinase families Ppk1 and Ppk2) and a phosphatase (Ppx), only a few proteins are known to functionally interact with polyP in bacteria(1, 3). These include enzymes that have been shown *in vitro* to be able to use polyP as a substrate for phosphorylation reactions, such as NAD kinases and glucokinases(1, 3). In addition, several proteins containing a positively-charged **C**onserved **H**istidine **α**-helical **D**omain (CHAD), have been shown by microscopy to localize to polyP granules(4). It may be that the specificity of binding to polyP is mediated by cooperative assembly of multicomponent protein complexes, making it difficult to understand polyP binding through binary interactions. Because polyP forms granular superstructures in many bacteria, co-localization studies can serve as a powerful method to identify true polyP-interacting proteins.

50 We and others have observed that polyP granules are organized within cells, raising the possibility
51 that the subcellular localization of these structures is a regulated process(5–8). An important
52 motivation for characterizing the polyP granule proteome is therefore to identify not just polyP-utilizing
53 proteins, but those that specifically contribute to the formation and organization of these structures. In
54 *P. aeruginosa*, polyP granules become transiently evenly spaced on the long axis of the cell during
55 nitrogen starvation. In addition to the even-spacing phenomenon, a notable structural feature of polyP
56 granules is that they form in the nucleoid region of the cell, where the chromosome resides. PolyP
57 granules appear to affect chromosome function, as *P. aeruginosa* cells that cannot make polyP are
58 deficient in exiting the cell cycle during starvation, and these cells also have an elevated SOS DNA
59 damage response(9). PolyP also affects cell cycle progression in *Caulobacter crescentus*(10).
60 Moreover, in *C. crescentus*, it has been shown that disrupting cell cycle progression can in turn alter
61 granule organization (*C. crescentus* cells typically have 1-2 granules, which form and localize to the
62 quarter-cell position during cell cycle progression)(5). Taken together, these observations suggest that
63 polyP granules may be structurally and functionally linked to the chromosome. How and why polyP is
64 connected to bacterial chromatin remains to be explored, but the proteome of polyP granules may
65 provide clues.
66
67 In this study, our goal was to develop a polyP granule enrichment protocol in *P. aeruginosa* strain
68 UCBPP_PA14 (herein referred to as just “PA14”) as a screening tool to characterize the polyP
69 granule associated proteome. We then validated our protocol by confirming that one of our candidate
70 proteins from this screen, AlgP, indeed localizes to granules. AlgP is a histone H1-like putative DNA
71 binding protein that has a predicted intrinsically disordered C-terminal domain containing tandem
72 repeats of KPAA residues(11, 12). We found that the C-terminus of AlgP is required for granule
73 spacing but that AlgP does not play a role in efficient cell cycle exit during nitrogen starvation. Our
74 proteomic screen represents the first step in determining the interactome of polyP in the opportunistic
75 human pathogen *P. aeruginosa*, and hopefully other bacteria in the future.

76

77 **RESULTS**

78 **PolyP granule enrichment and proteomic analysis.**

79 We developed a protocol for enrichment of polyP granules and analysis of granule-associated
80 proteins. We had two objectives when choosing a culture condition for granule isolation: (1) a
81 condition in which polyP granules are evenly spaced, because we are interested in identifying protein
82 factors that may contribute to spatial positioning of granules, and (2) a condition where polyP granules
83 are abundant, and the presence of polyhydroxyalkanoate (PHA) granules is minimized, to avoid
84 cross-contamination by proteins associated with PHA granules. Three hours of nitrogen starvation in
85 minimal medium satisfied both of these criteria, as shown in our previous work(9). Briefly, we
86 fractionated a lysate of WT and a ∆polyP strain (a quadruple knockout of *ppk1*, *ppk2A*, *ppk2B*, and
87 *ppk2C*) by ultracentrifugation in a self-forming Percoll gradient(13)(Fig 1A). We observed a brownish-
88 yellow pellet at the bottom of the WT gradient, but not the ∆polyP gradient (Fig 1B). We extracted
89 proteins from the pellet and whole lysate of WT and subjected them to label-free proteomic analysis
90 (see Materials and Methods for details).

91

92 We identified approximately 1200 proteins in the pellet fraction. Average protein abundances for the
93 pellet and lysate from three independent experiments are shown in Figure 1C. As an initial verification
94 for extraction methodology, we sought to confirm enrichment of known polyP associated proteins,
95 including the previously mentioned polyP kinases (Ppk1, Ppk2A, Ppk2B, and Ppk2C),
96 exopolyphosphatase (Ppx), and two CHAD-containing proteins (PA14_13320 and PA14_26940).
97 Ppk1 was more abundant in the lysate than in the pellet and Ppk2B was not detected in our screen.
98 Ppk2C was enriched and highly abundant in the pellet fraction. Ppk2A was detected in the pellet
99 fraction in one of three replicates with low abundance. Ppx was present in the lysate fraction only.
100 One of the CHAD-containing proteins, PA14_26940, was consistently detected in the pellet fraction
101 but PA14_13320 was not. We note that some ribosome-associated proteins were more abundant and

102 enriched in the pellet than lysate. However, we excluded this class from subsequent analysis, as they
103 are known to easily extract under the salt conditions used for our screen(14).
104
105 We hypothesized that our granule proteomic screen would identify two broad but non-exclusive
106 classes of proteins: (1) structural proteins that contribute to polyP granule formation, and (2) client
107 proteins that use polyP for another function, such as kinases that use polyP for phosphorylation
108 reactions. PolyP has one of the highest charge densities of any macromolecule in the cell(15). Hence,
109 we decided to focus initially on the first class, which we reasoned would have two key characteristics:
110 high enrichment and positive charge. A plot of enrichment, defined as the ratio of abundance of
111 protein in pellet to the lysate, versus the abundance is shown in Fig 1D. Ppk2C was one of the nine
112 highly enriched and abundant enriched protein candidates identified in this step. A plot of net protein
113 charge at pH 7 (obtained from the Pseudomonas Genome Database (16)) versus protein enrichment
114 in the polyP pellet is shown in Figure 1E, revealing one protein, AlgP, that distinctly stood out due to
115 its net charge of +55. In contrast, PhaF, which is a polyhydroxyalkanoate (PHA) granule associated
116 protein with a net positive charge +35 was abundant, but not enriched per our screening criteria. AlgP
117 and PhaF share a highly homologous C-terminal domain enriched in closely-spaced lysine residues
118 (see Discussion), and their abundance is therefore likely an underestimate due to the trypsin cleavage
119 treatment for mass spectrometry. Based on these abundance, enrichment, and physiochemical
120 criteria, we decided to focus on AlgP for subsequent analysis.
121
122 **AlgP localizes to polyP granules**
123 We used fluorescence microscopy to assess whether AlgP is enriched in polyP granules, as our
124 proteomic analysis suggests. We replaced the endogenous copy of AlgP in the genome with N and C-
125 terminally tagged fluorescent chimeras of AlgP with mApple. AlgP-mApple forms small irregular
126 puncta and patches in exponentially growing cells (Fig 2A, top left). After 3h of nitrogen starvation,
127 AlgP-mApple forms discrete evenly spaced puncta on the long axis of the cell (Fig 2A, bottom left).

128 Total fluorescence of AlgP-mApple revealed that AlgP is expressed during exponential growth and
129 increases in abundance during starvation (Fig 2B).
130
131 We then used DAPI staining to compare the localization of these puncta with polyP granules, and
132 qualitatively observe clear co-localization (Fig 2C, top panels). Demographs of the relative position of
133 DAPI and AlgP-mApple-labeled foci on the long axis of the cell reveal a similar banding pattern
134 between the two fluorescent channels (Fig 2D). We compared the number and positioning of DAPI-
135 labeled polyP granules in WT versus AlgP-mApple cells, for all foci-containing cells, to determine if
136 the chimeric fusion interferes with granule biogenesis. To determine whether the even spacing
137 granule phenotype we have previously observed is preserved in AlgP-mApple-labeled cells, and to
138 quantify co-localization of DAPI and AlgP-mApple labeled foci, we examined the normalized relative
139 position of foci on the long axis of the cell in both channels, for both 2-foci and 3-foci cells (Fig 2E, F).
140 We observed even spacing in both channels, and the position of individual foci in the two channels
141 was positively correlated in the scatter plot. We also compared the number of foci per cell in cells
142 expressing AlgP-mApple with that of WT, again for all foci-containing cells. We observed a similar
143 fraction of cells with 1 DAPI-labeled foci in WT and AlgP-mApple cells (Fig 2G), but slightly more 2
144 DAPI-labeled foci in WT than AlgP-mApple cells, and slightly fewer >2 DAPI-labeled foci in WT than
145 AlgP-mApple cells (Fig 2H, I). The fraction of mApple-labeled foci per cell was similar to DAPI-labeled
146 foci for 2-foci cells, though we observed slightly fewer 1 mApple-labeled foci than 1 DAPI foci per cell,
147 and slightly more >2 mApple-labeled foci than >2 DAPI labeled foci (Fig 2G-I, summarized in Table
148 S3a).
149
150 The mApple-AlgP chimera resulted in a different behavior. The total fluorescence intensity of this
151 protein was significantly lower both in exponential growth and during starvation, suggesting that the N-
152 terminal tag may interfere with expression, folding, or stability of the full-length protein (Fig 2B). The
153 localization of mApple-AlgP was different from AlgP-mApple: we still observed puncta, but significantly

154 fewer than we observed with the C-terminal tag (Fig 2A, right panels). The mApple-AlgP protein co-
155 localize with granules, but granule number and organization are significantly perturbed (Fig 2C,
156 bottom panels, D, G). Together these observations suggested that AlgP might play a role in the
157 subcellular positioning of polyP granules.
158

159 **AlgP affects granule maturation and spatial organization**

160 AlgP is a 352 amino acid (aa) protein with a 105aa N-terminal domain predicted to be α-helical
161 (Phyre2), and a 195aa predicted intrinsically disordered C-terminal domain containing a 154aa region
162 of tandem repeats of KPAA(17). There are 25 perfect KPAA repeats interspersed with variants,
163 including 7 KPVA, 4 KTAAA, one KPAV, and two alanine spacers. Two KPAA repeats fall outside of
164 this 154aa contiguous region (Fig 3A and S2). To determine if AlgP is required for polyP granule
165 formation and/or organization, we constructed a clean deletion *(Δ*algP*)*. Granule number and spatial
166 organization is perturbed in Δ*algP* cells (Fig 3B, C). We performed complementation analysis by
167 inserting a copy of *algP* under its native promoter at the *att*Tn7 locus, and observed partial rescue of
168 granule number and organization (Fig S3). Given the limits of light microscopy to detect small
169 granules and to accurately measure granule size, we used TEM as an orthogonal method to
170 characterize the granule phenotype in Δ*algP* cells early in starvation (1.5h) and at 3h. We observed
171 fewer, larger granules for Δ*algP* cells at both timepoints (Fig 4A-C). While granules were larger in
172 Δ*algP* cells than WT cells at 1.5h, we saw a larger subpopulation of cells without granules at this
173 timepoint in Δ*algP* cells (26% of ΔalgP cells versus 2% of WT cells). Even including these 'zero-
174 volume' cells in the distribution, the average volume of granules for Δ*algP* cells was still larger than for
175 WT cells. Indeed, when we look at the volume of the largest granule per cell, this trend towards larger
176 granules becomes very apparent, (Fig 4D). While the distribution of granular volume is different in
177 Δ*algP* cells, with fewer, larger granules, the loss of AlgP does not appear to lead to a net decrease in
178 the total volume of polyP granules per cell. We see a broader distribution of total granular volume per

179 cell Δ*algP* cells than in WT cells (Fig 4E). Summary statistics for TEM quantification are provided in
180 Table S3b.
181
182 We note that for the TEM analysis we observe a subpopulation of cells with many small 'satellite'
183 granules. We previously observed these small granules of 59 ± 20 nm nanometers in diameter, or
184 smaller, appear only in a fraction of cells(9). We did not quantify these 'satellite' granules in our
185 analysis, but we note the fraction of cells that contain them: in 3h nitrogen-starved cells, we observe
186 these in 24% of WT cells and 26% of Δ*algP* cells. We show examples of cells with 'satellite' granules
187 in Fig S4A.
188
189 **Deletion of the KPAA repeat domain results in loss of granule positioning**
190 The C-terminal 154-amino acid KPAA repeat domain of AlgP is highly homologous to the C-terminus
191 of PhaF. In PhaF, this domain is thought to bind DNA and tether polyhydroxyalkanoate (PHA)
192 granules to the nucleoid and thus contribute to their even distribution within cells. To determine if the
193 KPAA-repeat domain of AlgP plays a role in granule spacing, we generated an AlgP truncation mutant
194 where we removed the last 195 C-terminal amino acids (residues 157-352, including the 154aa repeat
195 region, Fig 3A, S2), In this *algP*ΔCTD strain, we observe a similar decrease in granule number per cell
196 as with Δ*algP* cells (Fig 3A-C). Qualitatively we also observe this decrease in granule number by TEM
197 (Fig 4A, right panels) though we have not quantified this effect in the *algP*ΔCTD strain for the TEM
198 data.
199
200 **AlgP localization depends on polyP kinases**
201 In the absence of starvation, we noticed that AlgP-mApple is not diffuse, but already forms puncta (Fig
202 2A). These puncta might form due to interactions with the chromosome, or with a specific polyP
203 kinase, or nascent polyP granules. Indeed at 0h we observed small putative nascent granules by
204 TEM, though their presence in growing cells is variable (examples shown in Fig S4B). To determine

205 whether AlgP localization is tied to the polyP polymer itself or instead to the polyp kinases, we
206 expressed our AlgP-mApple fusion in various *P. aeruginosa* strains lacking some or all of the kinases.
207 A mutant lacking all four polyP kinases lacks these puncta, suggesting that the localization depends
208 on polyP and/or specific polyP kinases (Fig 5A). We note that in ∆polyP cells, we occasionally
209 observe cells with a single DAPI stained puncta (<10% of cells), with which AlgP-mApple co-localizes.
210 We do not believe these puncta are polyP granules because of their small size and number per cell,
211 and because we do not see them by TEM (Fig 4A). We can only speculate about what they might
212 represent, acknowledging that dyes can act non-specifically and DAPI is known to undergo a red
213 emission shift when bound to RNA as well as other biomolecules(18). We next sought to determine
214 whether the AlgP-mApple puncta we observe depend on the polyP polymer, or one of the polyP
215 kinases specifically. We previously showed that either Ppk1 or Ppk2A is sufficient for granule
216 biogenesis(9). In a ∆*ppk2a*∆*ppk2b*∆*ppk2c* triple mutant, we observe puncta formation, indicating that
217 Ppk1 alone is sufficient for AlgP-mApple puncta formation (Fig 5A, 3rd column). Similarly, in a
218 ∆*ppk1*∆*ppk2b*∆*ppk2c* triple mutant, we observe puncta formation, indicating that Ppk2A alone is also
219 sufficient (Fig 5A, right panels).
220
221 We then looked at co-localization of AlgP-mApple with Ppk2A. We previously showed that Ppk2A-
222 mCherry can co-localize with DAPI-labeled polyP granules(9). We qualitatively observe co-localization
223 of Ppk2A-mNeonGreen with AlgP-mApple, although the Ppk2A-mNeonGreen and Ppk2A-mCherry
224 signals are low when these proteins are expressed from the native *ppk2A* promoter and not every
225 DAPI-stained or AlgP-mApple-labeled granule has visible Ppk2A fluorescence (Fig 5B). We conclude
226 that AlgP-mApple is a brighter and more consistent marker of granules than Ppk2A-mNeonGreen.
227
228 Finally, we noticed that the AlgP-mApple fluorescence in ∆polyP cells was not completely diffuse
229 throughout the cytoplasm (Fig 5A, 5C). Instead, we observed apparent co-localization of AlgP-mApple
230 with the nucleoid region of the cell, as visualized by Sybr Green staining, suggesting that in ∆polyP

231 cells, AlgP may bind nonspecifically to DNA (Fig 5C). Together these data suggest that AlgP-mApple
232 puncta formation depends not on a specific polyP kinase, but rather the presence of small amounts of
233 polyP in growing cells, and that AlgP may bind to the chromosome more broadly in the absence of
234 polyP.
235

236 **AlgP is not required for efficient cell cycle exit**

237 We previously showed that polyP is required for efficient cell cycle exit in response to nitrogen
238 starvation(9). We also previously showed that transient even spacing of granules on the long axis of
239 the cell coincides with the period of cell cycle exit, between 3 and 6 hours into nitrogen starvation(9).
240 We therefore wondered whether AlgP, which is required for granule organization, might also affect
241 efficient cell cycle exit. To characterize the effect of AlgP on cell cycle exit, we used fluorescent
242 markers to label the chromosomal origin of replication and open DNA replication forks, as we have
243 done previously. Briefly, we labeled open DNA replication forks with a fluorescent chimera of single
244 stranded DNA binding protein (SSB-mCherry), and we used the heterologous chimeric chromosome
245 partitioning protein GFP-ParB^{pMT1} and its cognate DNA binding sequence *parS*^{pMT1} to label the
246 chromosomal origins. In exponential growth, most WT and ΔpolyP cells are copying their
247 chromosomes, with more than one origin/cell and an open DNA replication fork (Fig 6B,C,
248 summarized in Table S3c). While we observe a similar fraction of cells with open forks in
249 exponentially growing Δ*algP* cells, the fraction of cells with more than one origin per cell is significantly
250 lower. However, the bulk growth rates of the WT and Δ*algP* are similar (Figure S5), suggesting that
251 the difference we observe with the fluorescent tags does not reflect an underlying replication defect.
252 At six hours after shifting exponentially growing cells to nitrogen-limited MOPS minimal media, 10±6%
253 of WT and 13±5% of Δ*algP* cells have more than one origin per cell, and 3±2% of WT and 2±2% of
254 Δ*algP* cells have open DNA replication forks (Fig 6B). In contrast, as we previously have shown,
255 ΔpolyP cells have a defect in efficient exit, as 87±4% still had more than one origin/cell and 35±3%

256 had open forks after 6 hours of nitrogen starvation (Fig 6B,C, summarized in Table S3c). These data
257 suggest that AlgP does not play a role in efficient cell cycle exit during nitrogen starvation.
258

259 **DISCUSSION**

260 We and others have observed spatial organization of polyP granules in bacteria, and further
261 hypothesized that polyP granules may have an organizational role(5, 19–22). Our granule enrichment
262 protocol led us to identify and validate the protein AlgP as a *bona fide* polyP associated protein. We
263 have also shown that AlgP has a structural role in granule formation: cells lacking AlgP or the C-
264 terminal domain of AlgP lack evenly spaced granules. How AlgP promotes even spacing of granules
265 remains to be determined, but the amino acid sequence of its C-terminus, along with previous studies
266 of AlgP and related proteins, provide exciting clues.
267

268 **Proteomic Screen: Proof of principle and next steps.**

269 PolyP has been implicated in diverse roles in bacterial cell physiology, but the identity and function of
270 the proteins that interact with this structurally simple biomolecule *in vivo* have remained elusive.
271 Previous studies have reported isolation of a polyP pellet obtained from centrifugation of lysates in
272 other bacteria including *Desulfovirbiro gigas, Corynebacterium glutamicum*, *and Ralstonia*
273 *eutropha*(23–25). In *R. eutropha*, these methods led to enrichment of known polyP kinases, confirmed
274 by fluorescence microscopy. To the best of our knowledge, the enrichment and characterization of
275 polyP granule-associated proteins has not been reported in *P. aeruginosa*.
276

277 Our granule enrichment protocol identified AlgP as a polyP-granule associated protein in *P.*
278 *aeruginosa* PA14. Here, the abundance and enrichment characteristics of two known classes of
279 polyP-associated proteins (polyP kinases and conserved histidine α-helical domain (CHAD) motif
280 containing proteins) are worth noting. *P. aeruginosa* has one known polyP phosphatase (ppx) and two
281 classes of polyP kinases: one Ppk1 and three Ppk2-type kinases (Ppk2a, Ppk2b and Ppk2C). In our

282 screen Ppk1 and Ppx were consistently depleted in the pellet fraction (Fig 1C). Although Ppk2A was
283 enriched in the pellet fraction at only low abundance and was detected in only one of three
284 independent experiments, Ppk2A-mNeonGreen colocalizes with polyP granule (Fig 5C). Hence it is
285 possible that Ppk2A weakly or transiently associated with polyP granules and that our granule
286 isolation protocol might have disrupted this association. Ppk2B was not detected in our screen but
287 Ppk2C was consistently and significantly enriched and abundant. Differential association of polyP
288 kinases and phosphosphotases with polyP granule has previously been observed in
289 betaproteobacterium *Rastlonia eutropha* H16: Ppk1A, Ppk2C, Ppk2D, and Ppk2E localize with the
290 polyP granule, whereas Ppk1B, Ppk2A, Ppk2B and Ppx are not associated with granules(4, 25).
291
292 Future work will seek to determine the co-localization characteristics of other proteins identified and
293 prioritized in our current screen. Recent work has reported that long-term nitrogen starvation in
294 *Escherichia coli* leads to the formation of large subcellular assemblies, like H-bodies and Hfq-foci,
295 which are a part of the RNA degradosome(26). Although these assemblies have not been reported in
296 starved *P. aeruginosa* cells, it is plausible that polyP could nucleate and mediate pelleting of these or
297 other unknown large bodies. The availability of AlgP as a granule marker will facilitate development of
298 improved granule fractionation and isolation protocols.
299
300 **Beyond alginate biosynthesis: A role for AlgP during starvation.** AlgP was previously identified
301 as a transcription factor thought to promote synthesis of alginate, an extracellular polysaccharide that
302 contributes to biofilm production and when overproduced results in a 'mucoid' phenotype in chronic
303 infections which correlates with a poor prognosis(27, 28)(29). The *algP* gene is adjacent *algR* and
304 *algQ*, known regulators of alginate biosynthesis. Recently, the putative role of AlgP in alginate
305 biosynthesis in *P. aeruginosa* has been called into question with the observation that deletion of *algP*
306 in two different mucoid strains of *P. aeruginosa*, did not result in a nonmucoid phenotype. In the Δ*algP*
307 mutant, alginate production was not attenuated and the alginate biosynthetic operon was not

308 affected(30). Our discovery that AlgP affects polyP granule localization demonstrates that this protein
309 remains important for starvation physiology. Although our AlgP mutant does not display a defect in
310 cell cycle exit, there are intriguing clues that it may play a role in modulating gene expression and
311 affect anaerobic survival(30). Indeed, AlgP was identified as highly expressed in the metabolically
312 less active regions of *P. aeruginosa* biofilms using BONCAT labeling, suggesting that starvation
313 upregulates its expression(31). In addition to localizing to granules, suggesting a direct structural role
314 in granule organization, it is also possible that AlgP modulates granule organization indirectly via its
315 effects on gene expression during starvation. While AlgP may not control alginate biosynthesis, polyP
316 and alginate, two polymers associated with fitness during starvation, may nevertheless share a
317 regulatory link. An older study implicated the transcriptional regulator AlgQ (originally called AlgR2) in
318 polyP biosynthesis(32). An Δ*algQ* mutant of *P. aeruginosa* has reduced levels of polyP, which can be
319 complemented either by adding back AlgQ, or one of its putative downstream effectors, nucleotide
320 diphosphate kinase (Ndk). The authors attribute the ability of Ndk to rescue polyP synthesis to its role
321 in modulating nucleotide pools, particularly GTP pools. GTP is required to make the stringent
322 response regulator (p)ppGpp, which was long thought to be required or polyP synthesis. More
323 recently, in both *E. coli* and *P. aeruginosa*, (p)ppGpp was found not to be required for polyP
324 synthesis(9, 33). Ndk may still influence polyP biosynthesis via its effect on nucleotide pools(9, 33).
325 Further work is necessary to explore the possible functional relationship between alginate and polyP,
326 both important biopolymers in starvation and pathogenesis.
327

328 **The C-terminus of AlgP: connecting polyP and bacterial chromatin.**

329 TEM and cryo-electron tomography of diverse bacterial species indicate that polyP granules tend to
330 form in the cell's nucleoid region(5–8). How and why these negatively charged polyanions associate
331 has remained unclear, but their colocalization suggests there may be a functional and/or structural
332 relationship between polyP granules and bacterial chromatin. While AlgP has not previously been
333 implicated in polyP granule biogenesis, the protein has long been thought to associate with the

334 nucleoid. The CTD of AlgP binds DNA, and peptides containing KPAA repeats bind DNA *in vitro*(27,
335 34). Molecular modeling studies suggest that the CTD may form a helix around DNA(34). A second
336 protein in *P. aeruginosa*, PhaF, contains a highly homologous CTD to AlgP and is also thought in
337 other Pseudomonads to bind DNA(35–37). PhaF has been shown to play a role in the organization of
338 another class of granular structures, polyhydroxyalkanoate (PHA) granules, which serve as a cellular
339 store of reduced carbon(35, 36). PhaF is thought to tether PHA granules to the chromosome, and in
340 its absence PHA granules clump together(36). The N-terminus of PhaF contains an amphipathic a
341 helix believed to interact with the hydrophobic surface of PHA granules, as well as an oligomerization
342 domain thought to drive tetramerization(35). The N-terminus of AlgP is predicted to be a helical but its
343 structure and function is not yet known.
344
345 In addition to the sequence homology to PhaF, AlgP has interesting similarities in terms of sequence
346 composition to the intrinsically disordered C-terminal tail of eukaryotic histone H1, also rich in lysine,
347 proline, and alanine, as has been previously noted(12, 27, 30). Unlike the other core histones which
348 are thought to have evolved from archaea, the histone H1 family is thought to be of bacterial
349 origin(38). Histone H1 in eukaryotes plays a role in chromatin condensation, and its CTD interacts
350 with linker DNA flanking the nucleosome(39). We observed that in the absence of polyP kinases, AlgP
351 appears to globally interact with the nucleoid. Further chromatin immunoprecipitation studies are
352 needed to understand its sequence preference *in vivo*. While the oligomeric state of AlgP is not yet
353 known, it is possible that the N-terminus might mediate higher order oligomers that are competent to
354 interact with both polyP and DNA.
355
356 **The C-terminus of AlgP: mediator of phase separation?**
357 A growing list of phase separated microcompartments have been observed in bacteria and are
358 thought to enable cells to achieve subcellular organization and generate specific microenvironments
359 in the absence of membrane-bound organelles(40, 41). Formation of such compartments is driven by

360 polyanions such as RNA, and intrinsically disordered proteins such as PopZ(42–46). Recently, polyP
361 has been shown to form liquid-like condensates with polycationic peptides and supercharged GFP
362 (+36GFP)(47–49). Additionally, the synthetic +36GFP-polyP condensates were shown to coalesce
363 and exhibit liquid-like properties in *Citrobacter freundii in vivo*(47). While we don't see a decrease in
364 total granular volume in Δ*algP* cells, as might be expected if the protein were critical for phase
365 separation of polyP granules, we do see a change in how polyP is distributed between granules, with
366 fewer, larger granules. We speculate that AlgP may normally function to limit granule fusion (Fig 7).
367 Fusion inhibition might occur by two mechanisms: non-specific or specific interactions of AlgP with
368 DNA when bound to small/nascent polyP granules could restrict their motion such that they can only
369 fuse with local granules tethered within a given chromatin neighborhood (Fig 7A). Such restriction to
370 fusing with local neighbors could lead to even spacing. Another non-exclusive model is that AlgP
371 changes the biophysical properties of granules in a manner that inhibits fusion, such as modulating
372 their surface charge. Future time-lapse imaging experiments of polyP granules are needed to address
373 these models. The fusion behavior of polyP granules in the Δ*algP* mutant in *P. aeruginosa* differs from
374 the fusion behavior of PHA granules in the Δ*phaF* mutant in another Pseudomonad, *Pseudomonas*
375 *putida*. In that species and strain, PHA granules bunch together but do not fuse, likely due to the
376 effect of another protein PhaI(36).
377

378 **Functional significance of AlgP in starvation fitness and pathogenesis**

379 Having discovered that AlgP modulates granule spacing in cells, the next important question is why
380 cells invest in granule spacing at all. Even spacing of another class of bacterial membraneless
381 compartments, carboxysomes, is important for the fitness of daughter cells and mediated by a
382 Brownian-ratchet mechanism(50, 51). While we don't yet understand the molecular mechanism fully
383 underpinning AlgP-mediated spacing, we now have the means in *P. aeruginosa* to disrupt polyP
384 granule organization and ask whether even spacing of polyP granules poses either a survival benefit

385 during starvation, or a growth advantage when nutrients become available. The CTD of AlgP has
386 been identified as a hotspot for genetic rearrangements in clinical isolates of *P. aeruginosa* from cystic
387 fibrosis patients(27, 52). These rearrangements alter KPAA repeat number, suggesting that this
388 domain is under selective pressure during chronic infections, however more research is needed to
389 determine whether there is a connection between these rearrangements and infection outcomes. The
390 consequences of these alterations in AlgP CTD domain length for granule biogenesis, starvation
391 fitness, and pathogenesis remain to be explored. Recently an alkyne derivative of the natural product
392 elegaphenone, which has antibiotic effects against *P. aeruginosa*, was shown to bind AlgP,
393 suggesting that AlgP is worthy of further exploration as a possible drug target(53).
394

395 **METHODS**

396 **Media and Growth conditions**

397 For nitrogen starvation experiments, strains were grown overnight at 37°C shaking in MOPS-
398 buffered minimal media (MMM): 40mM sodium succinate, 22mM NH_4Cl, 43mM NaCl, 2.2mM KCl,
399 1.25mM NaH_2P0_4, 1mM $MgSO_4$, 0.1mM $CaCl_2$, 7.5μM $FeCl_2 \cdot 4H_2O$, 0.8μM $CoCl_2 \cdot 6H_2O$, 0.5μM
400 $MnCl_2 \cdot 4H_2O$, 0.5μM ZnCl2, 0.2μM $Na_2MoO_4 \cdot 2H_2O$, 0.1μM $NiCl_2 \cdot 6H_2O$, 0.1μM H_3BO_3, and
401 0.01μM $CuCl_2 \cdot 2H_2O$, 50mM MOPS, pH 7.2). Optical density was determined at 500nm, rather
402 than 600nm, to minimize interference of pigments such as phenazines that *P. aeruginosa* produces
403 during starvation. 5mL subcultures at OD_{500} = 0.0125 to 0.025 were grown in glass test tubes at
404 37°C shaking at 250rpm to OD_{500} = 0.4 to 0.6, then spun down at room temperature for 5 minutes
405 at 5000xG, and resuspended to OD_{500} = 0.4 in nitrogen-limited MMM (Identical to MMM, but with
406 1mM NH_4Cl instead of 22mM) in clean glass test tubes and grown at 37°C shaking at 250rpm.
407 Time 0h = cells collected immediately before being spun down and shifted to nitrogen-limited
408 medium.
409

410 **Granule isolation and proteomic analysis**

411 Refer to the SI methods for a detailed description of cell culturing (cell growth and harvesting) and
412 proteomic analysis (sample preparation, data acquisition, software used and data availability). Briefly,
413 cells were grown to exponential phase at 37°C in MMM and then shifted to a low-nitrogen MMM for 3h
414 at 37°C. Cell pellets corresponding to 100mL of cell culture were flash frozen in liquid nitrogen. Pellet
415 was resuspended and incubated on ice for 15min in 1mL of lysis buffer, followed by microtip
416 sonication (Qsonica Q700), and additional nucleic acid digestion with Benzonase and DNAse I.
417 Lysate (0.5mL) was loaded onto 7mL pre-chilled Percoll gradient solution in ultracentrifuge tubes and
418 spun in a 50TI rotor at 21,300 RPM for 15 minutes. After removing the gradient solution, a Percoll-
419 encased pellet was resuspended in 1mL of dilution buffer and centrifuged in a tabletop
420 microcentrifuge at 10,000G for 2 min, resuspended, and the spin repeated to remove residual Percoll
421 from the pellet. The pellet was flash frozen in liquid nitrogen for subsequent proteomic analysis. The
422 (g/g) absolute mass fraction of a protein in a given sample was estimated using the spectral counting
423 technique(54). For a protein, its mass fraction abundance was tabulated by dividing the total number
424 its peptide-spectrum matches (PSM) by the total of all 14N PSMs in the sample. Enrichment of a
425 protein in our proteomics screen was defined as the ratio of the abundance of protein in the pellet to
426 the abundance in the lysate. See supplemental methods for more details.

427

428 **Plasmids and strains**

429 Strains, plasmids, and primers used in this study are listed in Tables S4a-c respectively. Strain
430 construction was performed as described previously, with details outlined in SI methods(9).

431

432 **Fluorescence microscopy**

433 All live cell imaging was acquired with a Nikon Ti2-E inverted microscope. Details of optical setup and
434 acquisition parameters are described in SI methods. Cells were imaged at 26°C on 1% agarose pads
435 containing MMM or MMM lacking ammonium chloride for nitrogen starvation experiments. Agarose

436 pads were imaged inside coverslip bottom dishes with plastic lids (Willco Wells, 0.17 mm/#1.5). For
437 DAPI-stained imaging of polyP granules, live cells were stained for 20 minutes in minimal media with
438 200μM DAPI from a 10 mM stock in dimethyl sulfoxide. DAPI staining of live cells for the purpose of
439 polyP granule imaging is not 100% efficient, with some cells not taking up enough dye to label
440 granules (to overcome this limitation of DAPI labeling, we used TEM to quantify the fraction of
441 granule-free cells). But DAPI can be used to characterize the number of granules per cell in cells that
442 take up the DAPI dye, and their organization. For Sybr Green staining, cells were stained for 20
443 minutes at 1X dye in minimal media before imaging.
444

445 **Transmission Electron Microscopy (TEM)**

446 Unfixed cells (3μL) were spotted onto glow discharged carbon-coated 200 mesh copper grids with
447 pinpointer grid (Ted Pella 01841-F) for 45 seconds, blotted with Whatman paper, and media salts
448 were washed off of grids by spotting the grids with 3uL of water and rapidly blotting; wash step was
449 repeated 5 times. Samples were analyzed at 120kV with a ThermoFisher Talos L120C transmission
450 electron microscope and images were acquired with a CETA 16M CMOS camera. TEM data was
451 plotted using iqplot: http://dx.doi.org/10.22002/D1.1614.
452

453 **Image analysis**

454 Cell segmentation and spot detection for fluorescence microscopy images was performed using
455 MicrobeTracker**(55)**. Spot detection was performed after rolling-ball background subtraction in ImageJ
456 (radius 10 pixels). Demographs of fluorescence intensity were constructed using the method and
457 script developed by Hocking et al., 2012**(56)**. For TEM imaging, granule number and diameter per cell
458 were measured manually using ImageJ as described previously**(9)**.
459

460 **Data availability**

461 The mass spectrometry proteomics data have been deposited and will be available upon publication
462 to ProteomeXchange Consortium via the UCSD's MassIVE repository with the accession codes:
463 MassIVE: MSV000087218 and ProteomeXchange: PXD025444
464 The raw light and electron microscopy data will be deposited upon publication to zenodo.org
465

466 **FIGURE LEGENDS**

467 **Figure 1. Workflow for isolation of polyphosphate granules from starved *P. aeruginosa* cells**
468 **and proteomic analysis. (A)** The workflow of granule isolation as described in the Methods section.
469 **(B)** The ultracentrifugation of a lysate from wild type *Pseudomonas aeruginosa PA14* cells in a Percoll
470 gradient solution generates a "pellet" fraction, which is not seen with a lysate from ∆polyP strain. The
471 bottom panel shows a zoomed-in view of the Percoll-encased pellet after discarding the Percoll
472 gradient solution. **(C-E):** Mass spectrometry analysis of the pellet fractions from three independent
473 experiments. **(C)** Absolute mass fraction of proteins in the "pellet" and "lysate", obtained from spectral
474 counting (see Methods and Fig S1) is shown in parts per million. The dashed diagonal corresponds to
475 a line of equal abundance in the pellet and lysate fraction. The data points below the diagonal line
476 correspond to proteins in higher abundance in the pellet fraction than in the lysate; diamond and
477 inverted triangle symbol marks the proteins identified in "lysate-only" and "pellet-only" fractions. (**D)**
478 The enrichment of proteins in the pellet plotted against the abundance of proteins in the pellet. The
479 cut-off of lines for enrichment are 8, (2^3, $\log_2$ fold-change =3) and abundance of 5000ppm. The highly
480 abundant and enriched proteins in the pellets are, therefore, located in the upper right quadrant. **(E)**
481 The calculated charge at neutral pH for proteins identified in the proteomics plotted against the fold
482 enrichment (negative charge cut-off for plotting is -75; refer to Fig S1c for the full plot). The horizontal
483 dashed line divides the data into positively and negatively charged proteins. For panels C-E: averages
484 of proteins identified in the mass spectrometric analysis from three independent experiments (light
485 gray circles); ribosomal-binding proteins (dark gray circles); AlgP(red circles); polyP kinases(blue

486 circles); polyhydroxyalkanoate granule-associated protein PhaF(green circles); and CHAD proteins
487 (orange circles).
488
489 **Figure 2: Subcellular localization of AlgP.** (A) Representative images of localization of AlgP-
490 mApple and mApple-AlgP translational fusion proteins. The genes encoding the chimeric proteins
491 replaced the endogenous *algP* at its native chromosomal locus. mApple fluorescence displayed in
492 magenta. Left panels: AlgP-mApple in exponential growth (0h) and after nitrogen starvation (3h).
493 Middle panels: mApple-AlgP displayed using the same contrast settings as for AlgP-mApple. Right
494 panels: the same mApple-AlgP images, shown with the higher contrast settings necessary to see
495 puncta. (B) Quantification of the average fluorescence intensity per cell (total intensity divided by the
496 area of the cell) for AlgP-mApple and mApple-AlgP in growing (0h) and nitrogen-starved (3h) cells. (C)
497 Localization of AlgP-mApple and mApple-AlgP relative to DAPI-stained polyP granules. mApple
498 fluorescence is displayed in magenta, DAPI fluorescence is displayed in yellow. Note that the contrast
499 settings in mApple channel are different for AlgP-mApple and mApple-AlgP because of different
500 brightness. They reflect the same settings used in the left panels of (A) for AlgP-mApple, and the
501 right panels of (A) for mApple-AlgP. (D) Demographs displaying the fluorescence intensity of DAPI
502 and mApple on the long axis of the cell in 3h nitrogen-starved cells. (E) Spatial organization of 2-foci
503 cells. Histograms display the normalized relative position on the long axis of the cell of the first foci in
504 blue and second foci in orange. The horizontal histogram (top) represents mApple foci, and the
505 vertical (left) histogram represents DAPI-labeled foci. Dots in the scatter plot show the correlation in
506 spatial position of mApple and DAPI foci. Grey dots represent foci found in one channel but not in the
507 other, these are also displayed as grey in the histograms. (F) Spatial organization of 3-foci cells. As in
508 (E), but the third foci is depicted in magenta. (G) Quantification of the fraction of 1-foci cells in the
509 population in both the DAPI and mApple channel. Note that 0-puncta cells are not included in these
510 calculations, because it is impossible to distinguish between cells that have no granules, and those in
511 which DAPI did not efficiently label the cell. The fraction of 1-foci cells therefore represents the ratio of

512 1-foci cells to all cells with 1 or more foci. Each point represents an independent replicate/day of
513 experiment. Dots represent results from independent experiments on different days, bar shows mean.
514 Variance analyzed using a one-way ANOVA. Significant differences between strains at the same time
515 point are marked with different uppercase letters based on a post hoc Tukey test (H) As in (G) but for
516 2-foci cells. (I) As in (G) but for cells with more than 2 foci. Scale bar: 2μm.
517
518 **Figure 3. Effect of AlgP and C-terminus of AlgP on localization of polyP granules during**
519 **nitrogen starvation.** (A) AlgP protein domain organization. AlgP contains an N-erminal 105aa
520 putative α-helical domain, predicted by Phyre2. The C-terminus contains a 195aa domain predicted to
521 be intrinsically disordered, with a 154 region of tandem repeats of KPAA. There are 25 perfect KPAA
522 repeats interspersed with variants, including 7 KPVA, 4 KTAAA, one KPAV, and two alanine spacers.
523 Two KPAA repeats that fall outside of this 154aa contiguous region. (B) Representative images of
524 DAPI-stained cells. (C) Demographs displaying the fluorescence intensity of DAPI on the long axis of
525 the cell in 3h nitrogen-starved cells. (D) Quantification of the fraction of DAPI-labeled cells in the
526 population with 1, 2, and >2 foci per cell. Each point represents an independent replicate/day of
527 experiment. Note that 0-puncta cells are not included in these calculations, because it is impossible
528 to distinguish between cells that have no granules, and those where DAPI did not efficiently label the
529 cell. The fraction of 1-foci cells therefore represents the ratio of 1-foci cells to all cells with 1 or more
530 foci. Dots represent results from independent experiments/days, the bar indicates the mean. Variance
531 analyzed using a one-way ANOVA. Significant differences between strains at the same time point are
532 marked with different uppercase letters based on a post hoc Tukey test. Scale bar: 2μm.
533
534 **Figure 4. Effect of AlgP and C-terminus of AlgP on number and size of polyP granules during**
535 **nitrogen starvation.** For the empirical cumulative distribution functions (ECDFs), the shading
536 represents confidence intervals for the ECDF acquired by bootstrapping. (A) Representative TEM
537 images of cells 1.5 and 3h after nitrogen starvation. (B) Distribution of the number of granules per cell

538 for WT and Δ*algP* cells at 1.5 and 3 hours into nitrogen starvation. (C) Distribution of volumes of all
539 individual granules at 1.5 and 3 hours into nitrogen starvation. (D) Distribution of volumes of the
540 largest granule per cell after 3 hours of nitrogen starvation. (E) Distribution of total granular volume
541 per cell (sum of volumes of all granules within a cell) after 3 hours of nitrogen starvation. Scale bar:
542 0.5μm.
543
544 **Figure 5. Effects of polyP kinases on AlgP and polyP granule localization after 3h of nitrogen**
545 **starvation.** (A) Localization of AlgP and DAPI-labeled puncta in the absence of all polyP kinases
546 (ΔpolyP), when only Ppk1 is present (3rd column), and when only Ppk2A is present (4th column). (B)
547 Localization of AlgP-mApple relative to Ppk2A-mNeonGreen. (C) Localization of AlgP relative to the
548 nucleoid in WT and ΔpolyP cells. The nucleoid was visualized using Sybr Green labeling (2nd row).
549 Scale bar: 2μm.
550
551 **Figure 6. Effects of AlgP on cell cycle exit during nitrogen starvation.** (A) Representative image
552 of WT exponentially-growing cells with chromosomal origins (green) and open DNA replication forks
553 (red). Origins are labeled using GFP-ParB^{pMT1} and a single copy of its cognate DNA binding site,
554 *parS^{pMT1}* DNA sequence at the *attB* locus, 19.5 kb from the origin. Forks are labeled using a
555 fluorescent chimera of single stranded DNA-binding protein (SSB-mCherry). We used a second copy
556 of the SSB promoter to drive both SSB-mCherry and GFP-ParB^{pMT1} expressed from the same operon,
557 and also integrated at the *attB* locus. (B) Fraction of cells with more than one chromosomal origin per
558 cell in growing (0h) or 6h nitrogen starved (6h) cells. Each point represents an independent
559 replicate/day of experiment. (C) Fraction of cells with at least one open DNA replication fork in
560 growing (0h) or 6h nitrogen-starved (6h) cells. Each point represents an independent replicate/day of
561 experiment. In (B) and (C), dots represent results from independent experiments/days, and the bar
562 indicates the mean. Variance was analyzed using a one-way ANOVA. Significant differences between

563 strains at the same time point are marked with different uppercase letters based on a post hoc Tukey
564 test. Scale bar: 2μm.
565
566 **Figure 7. Model for the role of AlgP in granule biogenesis.** (A) AlgP tethers nascent polyP
567 granules to the nucleoid, either through specific or non-specific contacts. Interactions between
568 nascent polyP granules and the nucleoid prevent free diffusion of granules, and lead to some degree
569 of local confinement within a chromosomal 'neighborhood.' Such confinement allows granules to fuse
570 only with their nearest neighbors on the timescale of granule maturation (hours). (B) Mature granules,
571 with their larger mass and more extensive interactions with the nucleoid, are more limited in their
572 radius of gyration and do not fuse with other granules, leading to even spacing.
573

574 **ACKNLOWLEDGEMENTS**

575 We thank Scott Henderson, Kimberly Vanderpool, and Theresa Fassel of the Core Microscopy Facility
576 at the Scripps Research Institute for their expert assistance in performing the TEM experiments. We
577 thank Megan Bergkessel, Ashok Deniz, Keren Lasker, Michael Manson, Dianne Newman, Daniel
578 Scholl and members of the Racki Lab for helpful feedback and discussions of this work. This work
579 was supported by the Donald E. and Delia B. Baxter Foundation (LRR), and
580 also in part by a grant from the NIH (R35-GM-136412 to JRW). Figures 1A and S1A were created with
581 BioRender.com.

REFERENCES

582 1. Rao NN, Gómez-García MR, Kornberg A. 2009. Inorganic polyphosphate: essential for growth and survival.
583 Annu Rev Biochem 78:605–647.

584 2. Denoncourt A, Downey M. 2021. Model systems for studying polyphosphate biology: a focus on
585 microorganisms. Curr Genet 67:331–346.

586 3. Kulakovskaya T, Kulaev I. 2013. Enzymes of Inorganic Polyphosphate Metabolism, p. 39–63. *In* Müller, WEG,
587 Wang, X, Schröder, HC (eds.), Biomedical Inorganic Polymers: Bioactivity and Applications of Natural and
588 Synthetic Polymeric Inorganic Molecules. Springer, Berlin, Heidelberg.

589 4. Tumlirsch T, Jendrossek D. 2017. Proteins with CHADs (Conserved Histidine α-Helical Domains) Are
590 Attached to Polyphosphate Granules In Vivo and Constitute a Novel Family of Polyphosphate-Associated
591 Proteins (Phosins). Appl Environ Microbiol 83:e03399-16.

592 5. Henry JT, Crosson S. 2013. Chromosome replication and segregation govern the biogenesis and inheritance
593 of inorganic polyphosphate granules. Mol Biol Cell 24:3177–3186.

594 6. Butan C, Hartnell LM, Fenton AK, Bliss D, Sockett RE, Subramaniam S, Milne JLS. 2011. Spiral Architecture of
595 the Nucleoid in Bdellovibrio bacteriovorus. J Bacteriol 193:1341–1350.

596 7. Takade A, Umeda A, Misumi T, Sawae Y, Amako K. 1991. Accumulation of phosphate-containing granules in
597 the nucleoid area of Pseudomonas aeruginosa. Microbiol Immunol 35:367–374.

598 8. Murata K, Hagiwara S, Kimori Y, Kaneko Y. 2016. Ultrastructure of compacted DNA in cyanobacteria by
599 high-voltage cryo-electron tomography. Sci Rep 6:34934.

600 9. Racki LR, Tocheva EI, Dieterle MG, Sullivan MC, Jensen GJ, Newman DK. 2017. Polyphosphate granule
601 biogenesis is temporally and functionally tied to cell cycle exit during starvation in *Pseudomonas aeruginosa*.
602 Proc Natl Acad Sci 114:E2440–E2449.

603 10. Boutte CC, Henry JT, Crosson S. 2012. ppGpp and polyphosphate modulate cell cycle progression in
604 Caulobacter crescentus. J Bacteriol 194:28–35.

605 11. Kato J, Chakrabarty AM. 1991. Purification of the regulatory protein AlgR1 and its binding in the far
606 upstream region of the algD promoter in Pseudomonas aeruginosa. Proc Natl Acad Sci 88:1760–1764.

607 12. Kato J, Misra TK, Chakrabarty AM. 1990. AlgR3, a protein resembling eukaryotic histone H1, regulates
608 alginate synthesis in Pseudomonas aeruginosa. Proc Natl Acad Sci 87:2887–2891.

609 13. Pertoft H, Laurent TC, Låås T, Kågedal L. 1978. Density gradients prepared from colloidal silica particles
610 coated by polyvinylpyrrolidone (Percoll). Anal Biochem 88:271–282.

611 14. Spitnik-Elson P, Atsmon A. 1969. Detachment of ribosomal proteins by salt: I. Effect of conditions on the
612 amount of protein detached. J Mol Biol 45:113–124.

613 15. Xie L, Jakob U. 2019. Inorganic polyphosphate, a multifunctional polyanionic protein scaffold. J Biol Chem
614 294:2180–2190.

615 16. Winsor GL, Griffiths EJ, Lo R, Dhillon BK, Shay JA, Brinkman FSL. 2016. Enhanced annotations and features
616 for comparing thousands of Pseudomonas genomes in the Pseudomonas genome database. Nucleic Acids Res
617 44:D646-653.

618 17. Kelley LA, Mezulis S, Yates CM, Wass MN, Sternberg MJE. 2015. The Phyre2 web portal for protein
619 modeling, prediction and analysis. Nat Protoc 10:845–858.

620 18. Omelon S, Georgiou J, Habraken W. 2016. A cautionary (spectral) tail: red-shifted fluorescence by DAPI–
621 DAPI interactions. Biochem Soc Trans 44:46–49.

622 19. Frank C, Jendrossek D. 2020. Acidocalcisomes and Polyphosphate Granules Are Different Subcellular
623 Structures in Agrobacterium tumefaciens. Appl Environ Microbiol 86:e02759-19.

624 20. Seufferheld M, Vieira MCF, Ruiz FA, Rodrigues CO, Moreno SNJ, Docampo R. 2003. Identification of
625 Organelles in Bacteria Similar to Acidocalcisomes of Unicellular Eukaryotes*. J Biol Chem 278:29971–29978.

626 21. Bode G, Mauch F, Ditschuneit H, Malfertheiner P. 1993. Identification of structures containing
627 polyphosphate in Helicobacter pylori. J Gen Microbiol 139:3029–3033.

628 22. Tocheva EI, Dekas AE, McGlynn SE, Morris D, Orphan VJ, Jensen GJ. 2013. Polyphosphate storage during
629 sporulation in the gram-negative bacterium Acetonema longum. J Bacteriol 195:3940–3946.

630 23. Jones HE, Chambers LA. 1975. Localized intracellular polyphosphate formation by Desulfovibrio gigas. J
631 Gen Microbiol 89:67–72.

632 24. Pallerla SR, Knebel S, Polen T, Klauth P, Hollender J, Wendisch VF, Schoberth SM. 2005. Formation of
633 volutin granules in Corynebacterium glutamicum. FEMS Microbiol Lett 243:133–140.

634 25. Tumlirsch T, Sznajder A, Jendrossek D. 2015. Formation of polyphosphate by polyphosphate kinases and
635 its relationship to poly(3-hydroxybutyrate) accumulation in Ralstonia eutropha strain H16. Appl Environ
636 Microbiol 81:8277–8293.

637 26. McQuail J, Carpousis AJ, Wigneshweraraj S. 2021. The association between Hfq and RNase E in long-term
638 nitrogen-starved Escherichia coli. Mol Microbiol Online ahead of print.

639 27. Deretic V, Konyecsni WM. 1990. A procaryotic regulatory factor with a histone H1-like carboxy-terminal
640 domain: clonal variation of repeats within algP, a gene involved in regulation of mucoidy in Pseudomonas
641 aeruginosa. J Bacteriol 172:5544–5554.

642 28. Okkotsu Y, Little AS, Schurr MJ. 2014. The Pseudomonas aeruginosa AlgZR two-component system
643 coordinates multiple phenotypes. Front Cell Infect Microbiol 20;4:82.

644 29. Konyecsni WM, Deretic V. 1990. DNA sequence and expression analysis of algP and algQ, components of
645 the multigene system transcriptionally regulating mucoidy in Pseudomonas aeruginosa: algP contains multiple
646 direct repeats. J Bacteriol 172:2511–2520.

647 30. Cross AR, Csatary EE, Raghuram V, Diggle FL, Whiteley M, Wuest WM, Goldberg JB. 2020. The histone-like
648 protein AlgP regulon is distinct in mucoid and nonmucoid Pseudomonas aeruginosa and does not include
649 alginate biosynthesis genes. Microbiology 166:861–866.

650 31. Babin BM, Atangcho L, van Eldijk MB, Sweredoski MJ, Moradian A, Hess S, Tolker-Nielsen T, Newman DK,
651 Tirrell DA. 2017. Selective Proteomic Analysis of Antibiotic-Tolerant Cellular Subpopulations in Pseudomonas
652 aeruginosa Biofilms. mBio 8:e01593-17.

653 32. Kim H-Y, Schlictman D, Shankar S, Xie Z, Chakrabarty AM, Kornberg A. 1998. Alginate, inorganic
654 polyphosphate, GTP and ppGpp synthesis co-regulated in *Pseudomonas aeruginosa:* implications for stationary
655 phase survival and synthesis of RNA/DNA precursors. Mol Microbiol 27:717–725.

656 33. Gray MJ. 2019. Inorganic Polyphosphate Accumulation in Escherichia coli Is Regulated by DksA but Not by
657 (p)ppGpp. J Bacteriol 201:e00664-18.

658 34. Medvedkin VN, Permyakov EA, Klimenko LV, Mitin YV, Matsushima N, Nakayama S, Kretsinger RH. 1995.
659 Interactions of (Ala*Ala*Lys*Pro)n and (Lys*Lys*Ser*Pro)n with DNA. Proposed coiled-coil structure of AlgR3
660 and AlgP from Pseudomonas aeruginosa. Protein Eng 8:63–70.

661 35. Maestro B, Galán B, Alfonso C, Rivas G, Prieto MA, Sanz JM. 2013. A new family of intrinsically disordered
662 proteins: structural characterization of the major phasin PhaF from Pseudomonas putida KT2440. PloS One
663 8:e56904.

664 36. Galán B, Dinjaski N, Maestro B, de Eugenio LI, Escapa IF, Sanz JM, García JL, Prieto MA. 2011. Nucleoid-
665 associated PhaF phasin drives intracellular location and segregation of polyhydroxyalkanoate granules in
666 Pseudomonas putida KT2442. Mol Microbiol 79:402–418.

667 37. Prieto MA, Bühler B, Jung K, Witholt B, Kessler B. 1999. PhaF, a polyhydroxyalkanoate-granule-associated
668 protein of Pseudomonas oleovorans GPo1 involved in the regulatory expression system for pha genes. J
669 Bacteriol 181:858–868.

670 38. Kasinsky HE, Lewis JD, Dacks JB, Ausló J. 2001. Origin of H1 linker histones. FASEB J 15:34–42.

671 39. Cutter AR, Hayes JJ. 2017. Linker histones: novel insights into structure-specific recognition of the
672 nucleosome. Biochem Cell Biol Biochim Biol Cell 95:171–178.

673 40. Abbondanzieri EA, Meyer AS. 2019. More than just a phase: the search for membraneless organelles in
674 the bacterial cytoplasm. Curr Genet 65:691–694.

675 41. Azaldegui CA, Vecchiarelli AG, Biteen JS. 2021. The emergence of phase separation as an organizing
676 principle in bacteria. Biophys J 120:1123–1138.

677 42. Ladouceur A-M, Parmar BS, Biedzinski S, Wall J, Tope SG, Cohn D, Kim A, Soubry N, Reyes-Lamothe R,
678 Weber SC. 2020. Clusters of bacterial RNA polymerase are biomolecular condensates that assemble through
679 liquid–liquid phase separation. Proc Natl Acad Sci 117:18540–18549.

680 43. Al-Husini N, Tomares DT, Bitar O, Childers WS, Schrader JM. 2018. α-Proteobacterial RNA Degradosomes
681 Assemble Liquid-Liquid Phase-Separated RNP Bodies. Mol Cell 71:1027-1039.e14.

682 44. Al-Husini N, Tomares DT, Pfaffenberger ZJ, Muthunayake NS, Samad MA, Zuo T, Bitar O, Aretakis JR,
683 Bharmal M-HM, Gega A, Biteen JS, Childers WS, Schrader JM. 2020. BR-Bodies Provide Selectively Permeable
684 Condensates that Stimulate mRNA Decay and Prevent Release of Decay Intermediates. Mol Cell 78:670-682.e8.

685 45. Lasker K, von Diezmann L, Zhou X, Ahrens DG, Mann TH, Moerner WE, Shapiro L. 2020. Selective
686 sequestration of signalling proteins in a membraneless organelle reinforces the spatial regulation of
687 asymmetry in Caulobacter crescentus. Nat Microbiol 5:418–429.

688 46. Saurabh S, Chong TN, Bayas C, Dahlberg PD, Cartwright HN, Moerner WE, Shapiro L. 2020. Modulation of
689 kinase activity within a bacterial membraneless organelle. bioRxiv 2020.08.09.232405.

690 47. Wang X, Shi C, Mo J, Xu Y, Wei W, Zhao J. 2020. An Inorganic Biopolymer Polyphosphate Controls
691 Positively Charged Protein Phase Transitions. Angew Chem Int Ed 59:2679–2683.

692 48. Boeynaems S, Holehouse AS, Weinhardt V, Kovacs D, Van Lindt J, Larabell C, Van Den Bosch L, Das R,
693 Tompa PS, Pappu RV, Gitler AD. 2019. Spontaneous driving forces give rise to protein−RNA condensates with
694 coexisting phases and complex material properties. Proc Natl Acad Sci 116:7889–7898.

695 49. Alshareedah I, Moosa MM, Raju M, Potoyan DA, Banerjee PR. 2020. Phase transition of RNA-protein
696 complexes into ordered hollow condensates. Proc Natl Acad Sci U S A 117:15650–15658.

697 50. Savage DF, Afonso B, Chen AH, Silver PA. 2010. Spatially ordered dynamics of the bacterial carbon
698 fixation machinery. Science 327:1258–1261.

699 51. MacCready JS, Hakim P, Young EJ, Hu L, Liu J, Osteryoung KW, Vecchiarelli AG, Ducat DC. 2018. Protein
700 gradients on the nucleoid position the carbon-fixing organelles of cyanobacteria. eLife 7:e39723.

701 52. Chung JCS, Becq J, Fraser L, Schulz-Trieglaff O, Bond NJ, Foweraker J, Bruce KD, Smith GP, Welch M. 2012.
702 Genomic Variation among Contemporary Pseudomonas aeruginosa Isolates from Chronically Infected Cystic
703 Fibrosis Patients. J Bacteriol 194:4857–4866.

704 53. Zhao W, Cross AR, Crowe-McAuliffe C, Weigert-Munoz A, Csatary EE, Solinski AE, Krysiak J, Goldberg JB,
705 Wilson DN, Medina E, Wuest WM, Sieber SA. 2019. The Natural Product Elegaphenone Potentiates Antibiotic
706 Effects against Pseudomonas aeruginosa - Angew Chem Int Ed Engl. 58(25):858108584.

707 54. Gao J, Friedrichs MS, Dongre AR, Opiteck GJ. 2005. Guidelines for the Routine Application of the Peptide
708 Hits Technique. J Am Soc Mass Spectrom 16:1231–1238.

709 55. Sliusarenko O, Heinritz J, Emonet T, Jacobs-Wagner C. 2011. High-throughput, subpixel precision analysis
710 of bacterial morphogenesis and intracellular spatio-temporal dynamics. Mol Microbiol 80:612–627.

711 56. Hocking J, Priyadarshini R, Takacs CN, Costa T, Dye NA, Shapiro L, Vollmer W, Jacobs-Wagner C. 2012.
712 Osmolality-dependent relocation of penicillin-binding protein PBP2 to the division site in Caulobacter
713 crescentus. J Bacteriol 194:3116–3127.

714

Figure 1

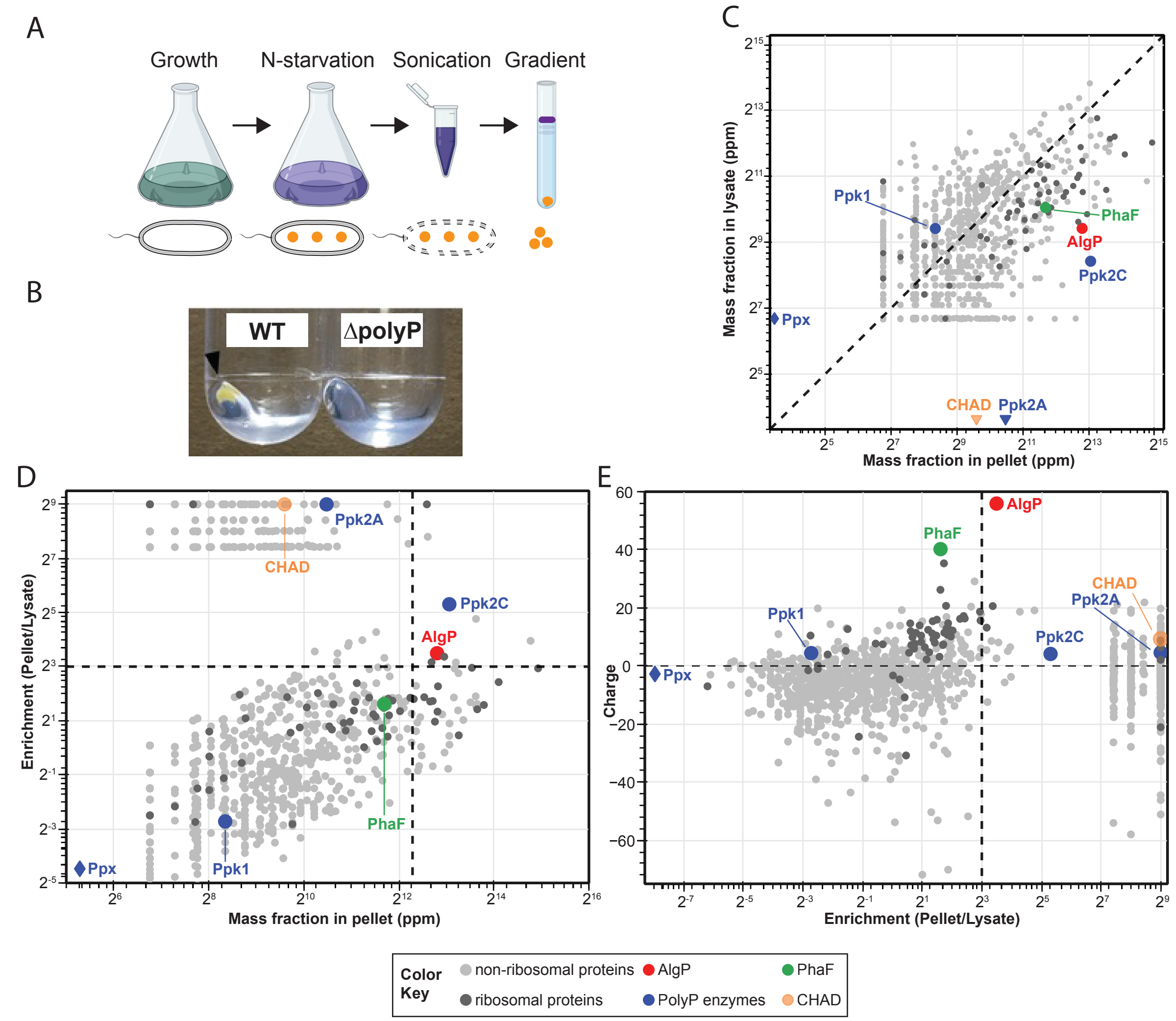
A
Growth
N-starvation
Sonication
Gradient
B
WT
ΔpolyP
C
Mass fraction in lysate (ppm)
Mass fraction in pellet (ppm)
Ppk1
PhaF
AlgP
Ppk2C
Ppx
CHAD
Ppk2A
D
Enrichment (Pellet/Lysate)
Mass fraction in pellet (ppm)
Ppk2A
CHAD
Ppk2C
AlgP
PhaF
Ppx
Ppk1
E
Charge
Enrichment (Pellet/Lysate)
AlgP
PhaF
CHAD
Ppk2A
Ppk1
Ppk2C
Ppx
Color Key
non-ribosomal proteins
ribosomal proteins
AlgP
PolyP enzymes
PhaF
CHAD

Figure 2

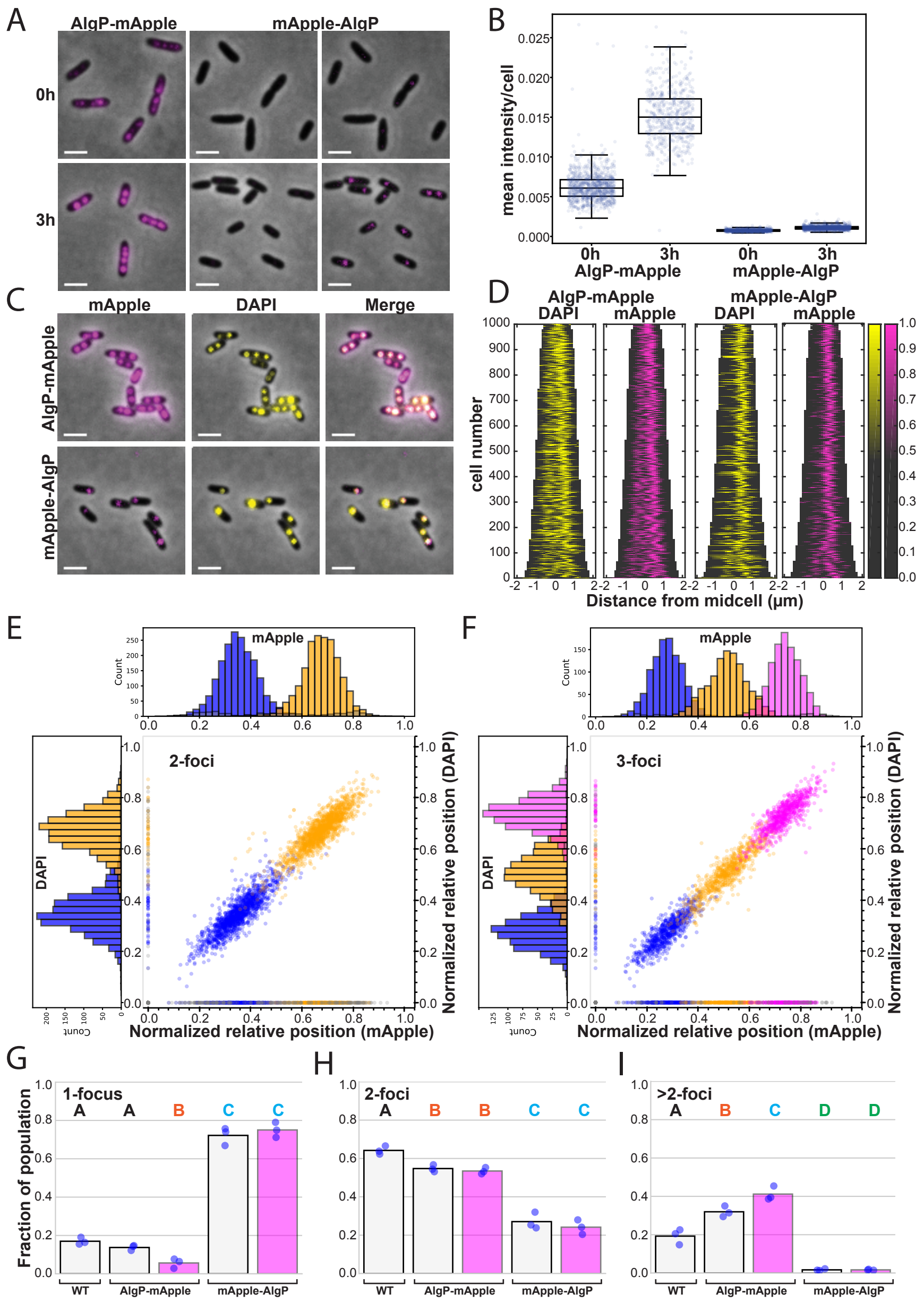
A
AlgP-mApple
mApple-AlgP
0h
3h
B
mean intensity/cell
0.025
0.020
0.015
0.010
0.005
0.000
0h
3h
0h
3h
AlgP-mApple
mApple-AlgP
C
mApple
DAPI
Merge
AlgP-mApple
mApple-AlgP
D
AlgP-mApple
mApple-AlgP
DAPI
mApple
cell number
Distance from midcell (μm)
E
mApple
Count
2-foci
DAPI
Normalized relative position (DAPI)
Normalized relative position (mApple)
F
mApple
3-foci
G
1-focus
Fraction of population
WT
AlgP-mApple
mApple-AlgP
H
2-foci
I
>2-foci

Figure 3

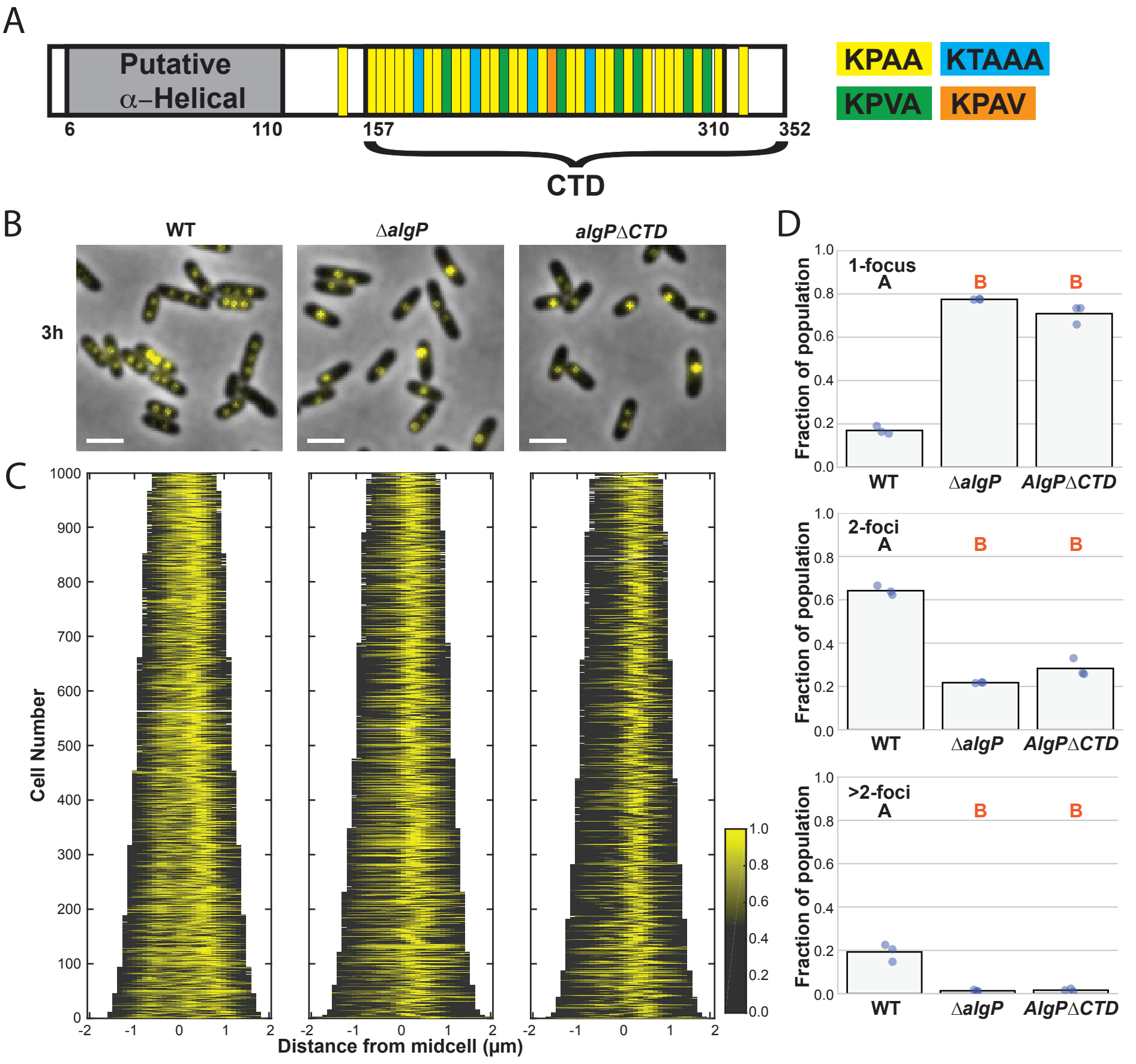
A
Putative
α–Helical
6
110
157
310
352
CTD
KPAA
KTAAA
KPVA
KPAV
B
WT
ΔalgP
algPΔCTD
3h
C
Cell Number
Distance from midcell (μm)
D
1-focus
2-foci
>2-foci
Fraction of population
WT
ΔalgP
AlgPΔCTD
A
B

Figure 4

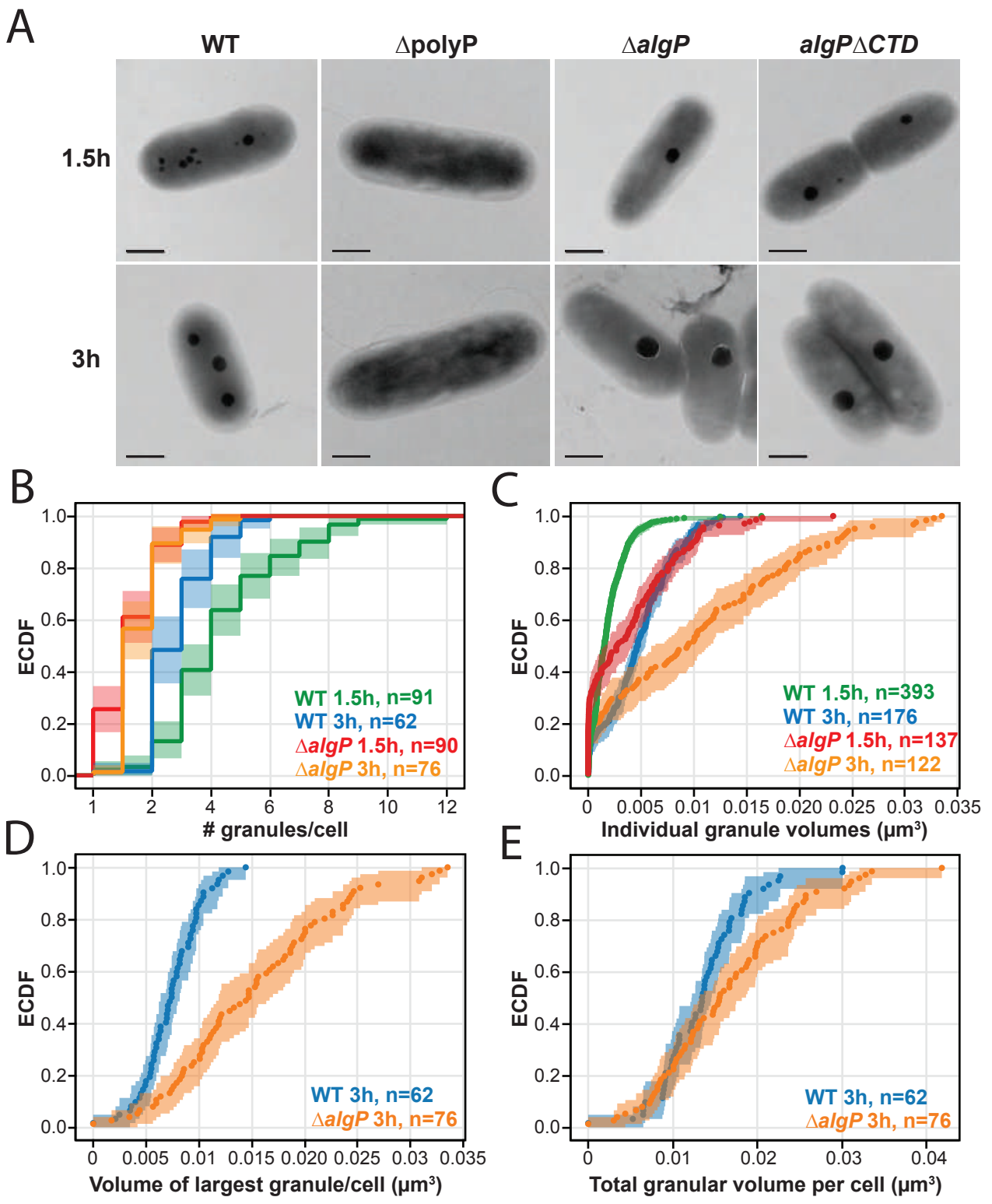
A
WT
ΔpolyP
ΔalgP
algPΔCTD
1.5h
3h
B
ECDF
WT 1.5h, n=91
WT 3h, n=62
ΔalgP 1.5h, n=90
ΔalgP 3h, n=76
C
ECDF
WT 1.5h, n=393
WT 3h, n=176
ΔalgP 1.5h, n=137
ΔalgP 3h, n=122
D
granules/cell
ECDF
WT 3h, n=62
ΔalgP 3h, n=76
Volume of largest granule/cell (μm³)
E
Individual granule volumes (μm³)
ECDF
WT 3h, n=62
ΔalgP 3h, n=76
Total granular volume per cell (μm³)

Figure 5

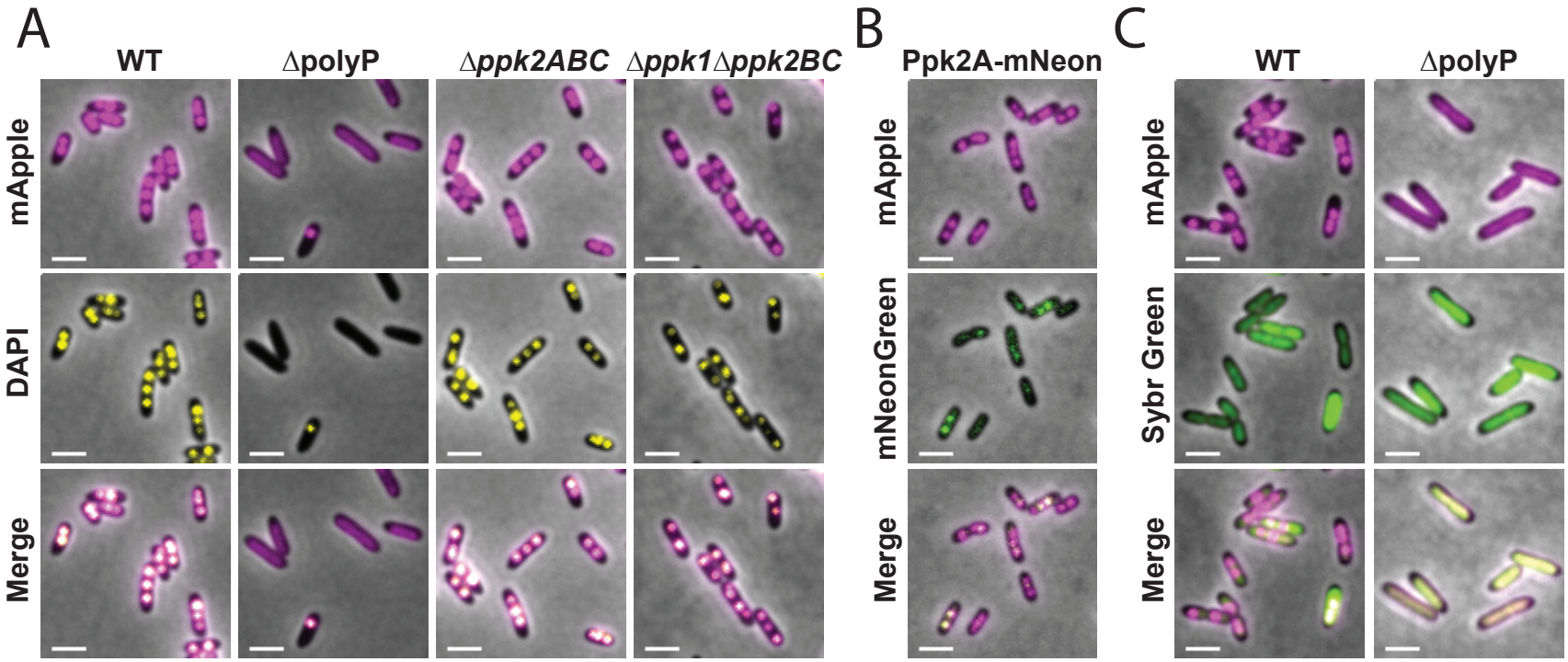
A
WT
ΔpolyP
Δppk2ABC
Δppk1Δppk2BC
mApple
DAPI
Merge
B
Ppk2A-mNeon
mApple
mNeonGreen
Merge
C
WT
ΔpolyP
mApple
Sybr Green
Merge

Figure 6

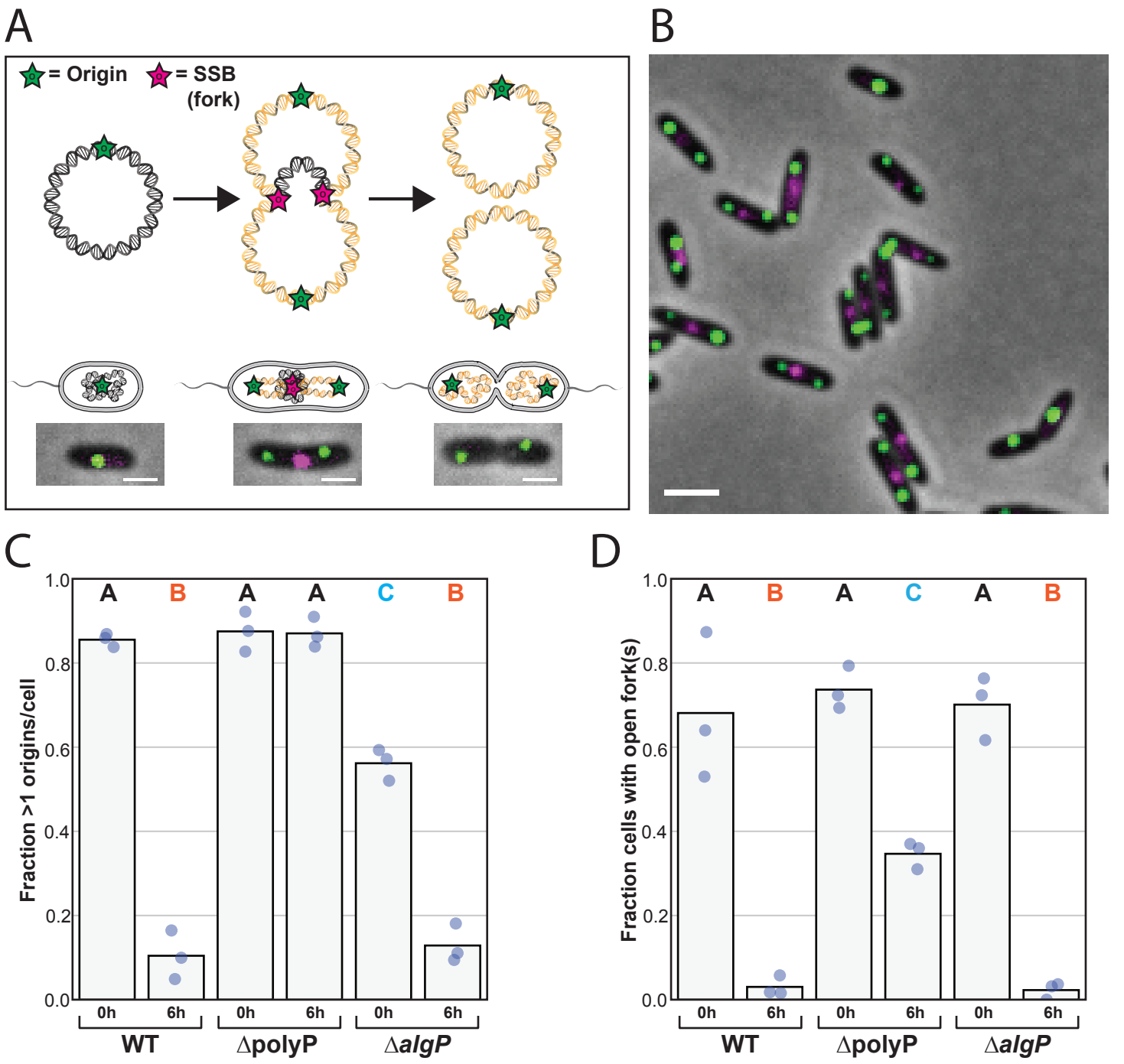
A
= Origin
= SSB (fork)
B
C
Fraction >1 origins/cell
1.0
0.8
0.6
0.4
0.2
0.0
A B A A C B
0h 6h 0h 6h 0h 6h
WT
ΔpolyP
Δ*algP*
D
Fraction cells with open fork(s)
1.0
0.8
0.6
0.4
0.2
0.0
A B A C A B
0h 6h 0h 6h 0h 6h
WT
ΔpolyP
Δ*algP*

Figure 7

A

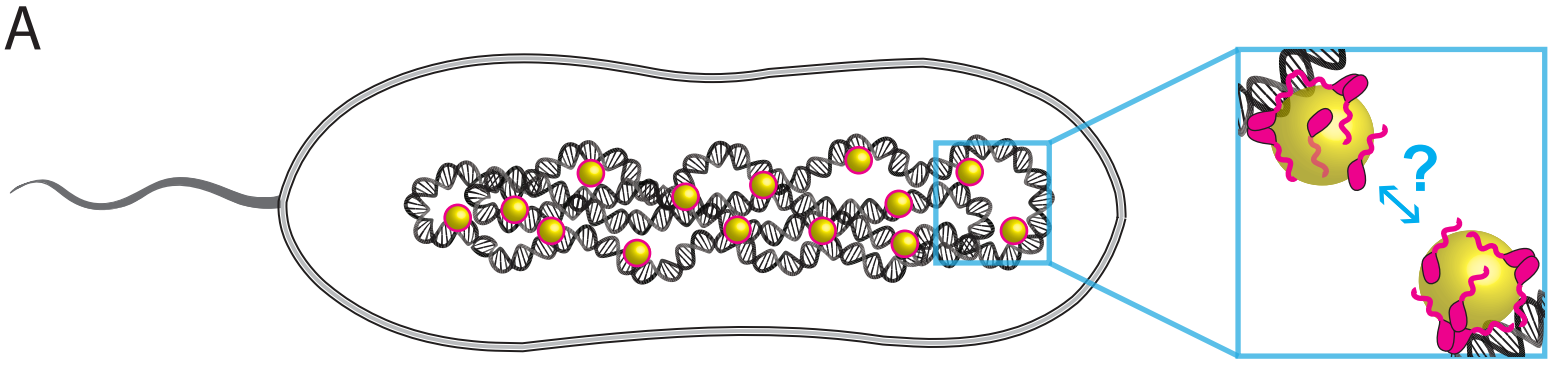
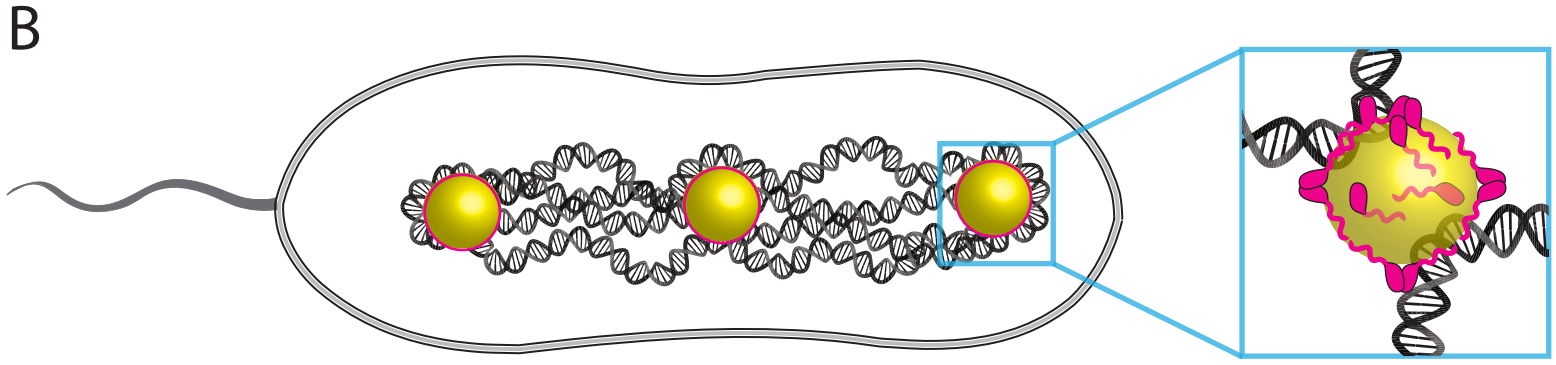
B